Exp Fluids (2014) 55:1713
DOI 10.1007/s00348-014-1713-9

RESEARCH ARTICLE

Oblique impacts of water drops onto hydrophobic and superhydrophobic surfaces: outcomes, timing, and rebound maps

C. Antonini · F. Villa · M. Marengo

Received: 8 October 2013 / Revised: 25 March 2014 / Accepted: 26 March 2014 / Published online: 8 April 2014

Abstract This paper presents an experimental study on water drop oblique impacts onto hydrophobic and superhydrophobic tilted surfaces, with the objective of understanding drop impact dynamics and the conditions for drop rebound on low wetting surfaces. Drop impact experiments were performed with millimetric water drops with Weber numbers in the range $25 < We < 585$, using different surfaces with advancing contact angles $111° < \theta_A < 160°$ and receding contact angles $104° < \theta_R < 155°$. The analysis of oblique impacts onto tilted surfaces led to the definition of six different impact regimes: deposition, rivulet, sliding, rolling, partial rebound, and rebound. For superhydrophobic surfaces, surface tilting generally enhanced drop rebound and shedding from the surface, either by reducing drop rebound time up to 40 % or by allowing drop rebound even when impalement occurred in the vicinity of the impact region. On hydrophobic surfaces, rebound was never observed for tilt angles higher than 45°.

C. Antonini and F. Villa have contributed equally to this study.

C. Antonini (✉) · F. Villa · M. Marengo (✉)
Department of Engineering, University of Bergamo, Viale Marconi 5, 24044 Dalmine, BG, Italy
e-mail: carlo.antonini@mavt.ethz.ch

M. Marengo
e-mail: m.marengo@brighton.ac.uk

C. Antonini
Laboratory of Thermodynamics in Emerging Technologies, Mechanical and Process Engineering Department, ETH Zurich, Sonneggstrasse 3, 8092 Zurich, Switzerland

M. Marengo
School of Computing, Engineering and Mathematics, University of Brighton, Cockcroft Building, C221, Lewes Road, Brighton BN2 4GJ, UK

1 Introduction

Water drop impacts onto solid substrates play a major role in a variety of industrial applications, including impact on combustion chamber wall inside engines (Dewitte et al. 2011), raindrop erosion (Abuku et al. 2009), turbine blade erosion (Li et al. 2008; Zhou et al. 2008), liquid spray cooling (Pasandideh-Fard et al. 2001), and ink-jet printing (Schiaffino and Sonin 1997). Investigation of the fundamental science of single drop impacts (Rioboo et al. 2001; Yarin 2006; Marengo et al. 2011) is the first step toward understanding and controlling liquid–solid interaction of complex phenomena, e.g., spray impacting on a solid wall, or ice accretion due to atmospheric supercooled water drops (Antonini et al. 2011).

In the last decade, an increasing interest has attracted researchers to investigate hydrophobic and superhydrophobic surfaces for their ability to repel liquid water (Liu et al. 2009; Quéré 2005) and increase drop mobility. In particular, on superhydrophobic surfaces, water drop repellency and mobility are high, thanks to a combination of high contact angles (i.e., the angles measured at the liquid–solid–gas interface) and low contact angle hysteresis. The high repellency is made possible by the presence of gas pockets trapped at the solid–liquid interface (Bhushan et al. 2009; Quéré 2005), limiting the contact between the liquid (in this case, water) and the solid. This wetting state is known as Cassie–Baxter (Fig. 1a), and differs to the Wenzel wetting state (Fig. 1b), in which the surface is completely wetted by the liquid (Reyssat et al. 2006; Bartolo et al. 2006). Transition between the two wetting states can be observed even in static conditions, e.g., due to pressure increase inside an evaporating drop (Papadopoulos et al. 2013, Antonini et al. 2014). In case of impacting drops, it has already been shown that at low impact speed

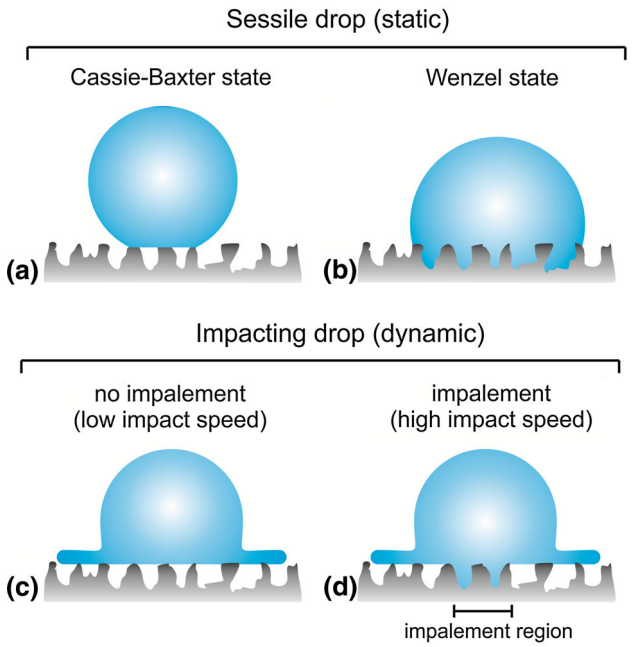

Fig. 1 Schematics of the different wetting state on an super hydrophobic surfaces, in static and dynamic conditions. A sessile drop on a surface can by in the **a** Cassie–Baxter state or in the **b** Wenzel state. When a drop impacts on a superhydrophobic surface: **c** at low impact speed, Cassie–Baxter state is conserved and no impalement is observed, whereas **d** at high impact speed, an area close to the impact zone switches to Wenzel state

(Reyssat et al. 2006; Bartolo et al. 2006) the Cassie–Baxter state can be preserved (Fig. 1c), so that drop will rebound after impact. However, for velocities higher than a critical value, which depends on surface properties, drop may not be able to rebound: according to the classical interpretation (Reyssat et al. 2006; Bartolo et al. 2006), in a region close to the impact zone, the wetting state changes from Cassie–Baxter to Wenzel state, due to local liquid penetration into the surface cavities, a phenomenon typically referred to as impalement (Fig. 1d).

The property of superhydrophobicity is attributed to surfaces having receding contact angles higher than 135° and contact angle hysteresis lower than 10°. Advancing and receding contact angles, θ_A and θ_R, respectively, are measured expanding and contracting quasi-statically a drop on a horizontal surface, and their difference, $\Delta\theta = \theta_A - \theta_R$, is the contact angle hysteresis. The contact angle threshold value is based on both experimental (Rioboo et al. 2012) and theoretical (Li and Amirfazli 2005) results.

On a horizontal superhydrophobic surface, drop rebound time, also known as contact time, was found by Richard et al. (2002) to be and function of drop mass, m, and liquid surface tension, σ, and independent from impact speed, V:

$$t_R = 2.6\left(\frac{\rho D_0^3}{8\sigma}\right)^{1/2} \quad (1)$$

where ρ is density and D_0 drop initial diameter. Interestingly, drop impact behavior and rebound time on a superhydrophobic surface are similar to the case of drop impact under Leidenfrost boiling conditions and on a sublimating substrate (Antonini et al. 2013a). Mao et al. (1997) studied impact on hydrophilic and hydrophobic surfaces with contact angles up to 97° and concluded that drop rebound can be observed on substrates showing an equilibrium contact angle higher than 90°. Rioboo et al. (2008) proposed a schematic drop impact regime map, identifying deposition, rebound, sticking, and fragmentation as possible outcome for drop impact on a horizontal surface. Antonini et al. (2013b) found that the receding contact angle θ_R is indeed the key wetting parameter to control drop rebound: up to $We = 585$, drop rebound was observed only on surfaces with receding contact angle θ_R higher than 100°; also, drop rebound time decreased by increasing receding contact angle, thus being minimized on superhydrophobic surfaces.

Although there is a long series of studies in the literature, which have analyzed normal drop impacts onto dry surfaces (Marengo et al. 2011), only few of them focused on oblique (i.e., non-normal) drop impacts. In Šikalo et al. (2005a, b) drop impact onto dry and wet tilted surfaces with contact angles ranging from 0° to 105° was studied. It was found that a drop typically deposits on the surface, but rebound can occur at high impact angles, i.e., almost tangential impacts, on both smooth and wetted surfaces; no rebound was observed for rough surfaces. Transition between deposition and rebound was found to be at constant critical normal Weber number ($We_{N,C} = 1$ for water on dry surface), where normal Weber number is calculated as $We_N = \rho D_0 V_N^2 / \rho D_0 V_N^2 \sigma . \sigma$, where V_N is the velocity component normal to the surface.

This paper represents the first systematic experimental study of oblique drop impact on hydrophobic and superhydrophobic surfaces, with the aim of identifying drop impact outcomes, defining impact regime maps, evaluating the drop rebound time, and finally, assessing the presence of the impalement condition on superhydrophobic surfaces.

2 Materials and methods

Water drops impacts were conducted on four different substrates: one hydrophobic surface, A1-Teflon, and two superhydrophobic surfaces, SHS-1 and SHS-2. All surfaces were characterized by means of sessile drop method, i.e., measuring the advancing, θ_A, and receding, θ_R, contact angles. A1-Teflon consists of a Teflon-coated glass (see

Table 1 Advancing, θ_A, and receding, θ_R, contact angles, contact angle hysteresis, $\Delta\theta$, and surface roughness, R, for tested surfaces

Surface	θ_A (°)	θ_R (°)	$\Delta\theta$ (°)	R (μm)
A1-Teflon	111	104	7	0.9
SHS-1	160	145	15	1.91
SHS-2	157	155	2	1.83

Maximum standard deviation for contact angles is ±3°. For the smooth hydrophobic sample, A1-Teflon, the reported roughness value is the root-mean-square surface roughness, measured using Atomic Force Microscope MFP-3D (Asylum Research). For superhydrophobic surfaces, SHS-1 and SHS-2, the reported roughness values correspond to mean surface roughness, measured using a roughness meter (Diavite DH-5, resolution 0.01 μm)

Huanchen et al. 2012, for more details). SHS-1 was fabricated on an aluminum substrate by aluminum etching in acid solution (to achieve the desired surface roughness) and subsequent spraying with Teflon® (10:1 v/v solution of FC-75 and Teflon® from DuPont™). SHS-2 sample was initially etched with hydrochloric acid at 37 % (Sigma-Aldrich) diluted 1:2 v/v with water for 2 min, at room temperature, and then rinsed with pure water and dried in air. Subsequently, the sample was immersed in a solution of 100 g of lauric acid [$CH_3(CH_2)_{10}COOH$, Sigma-Aldrich] and 1 l of ethanol (Sigma-Aldrich) at room temperature (12.7 % w/w concentration) for 2 h. During this process, hydrophobicity is imparted to the sample by grafting of lauric acid molecules on the substrate. Finally, the sample was rinsed with ethanol and dried in air. Table 1 reports the values of the advancing contact angles, θ_A, the receding contact angles, θ_R, and the contact angle hysteresis, $\Delta\theta$, together with the mean surface roughness.

For drop impact studies, a drop was generated at the tip of a needle, accelerated by gravity, and impacted on the dry solid surface. Experimental conditions were the following: drop impact velocity in the range $0.8 < V < 4.1$ m/s (±2 %), drop diameter $2.40 < D_0 < 2.60$ mm (±2 %), Weber number $We = \rho D_0 V^2/\rho D_0 V^2 \sigma.\sigma$ in the range $25 < We < 585$ (3.5 %), Ohnesorge number $Oh = \mu/\sqrt{\rho\sigma D_0}$ in the range $0.0021 < Oh < 0.0022$ (±1 %), surface advancing contact angle $111° < \theta_A < 160°$ (±3°), receding contact angle $104° < \theta_R < 155°$ (±3°), and surface tilt angle $15° < \alpha < 80°$ (±0.1°). The upper tilt angle limit, i.e. 80°, was set by the inability to capture entirely drop trajectory and dynamics after impact at higher surface tilt.

Drop impact images were recorded using a high-speed camera, PCO 1200-hs. To record drop impact events, images were taken from the side, with the same view as illustrated in Fig. 2: camera direction is perpendicular to the symmetry plane of the impacting drop. This view was chosen, since it allows measuring drop rebound time, the kinematics of the uphill and downhill points of the contact line, and the contact diameter $D_{//}$, measured in the same direction as the tangential velocity, V_T (Fig. 2). Images were manually analyzed to identify the drop impact outcome and to eventually measure drop rebound time, in case rebound occurs.

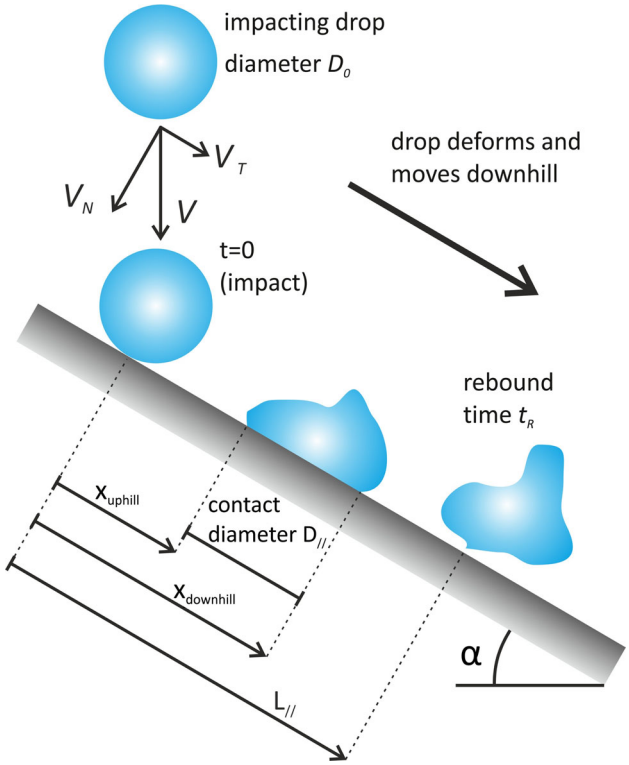

Fig. 2 Schematic of drop impact and evolution onto a tilted surface, with indication of most relevant impact parameters. Images were recorded with a frame rate from 1,015 to 3,000 fps and pixel resolution in the range 30–35 μm. All this visualization parameters represent the best compromise between spatial and temporal resolution, and field of view

3 Results and discussion

3.1 Drop impact outcomes

The first part of the study involved the identification of principal drop impact outcomes on tilted surfaces. Six main outcomes were identified in order to distinguish the phenomena occurring to the main part of the impacting drop. In fact, since no strong breakup was observed, it was always possible to individuate the evolution of the liquid bulk, neglecting the casual presence of secondary droplets. The following outcomes, illustrated in Fig. 3, were observed:

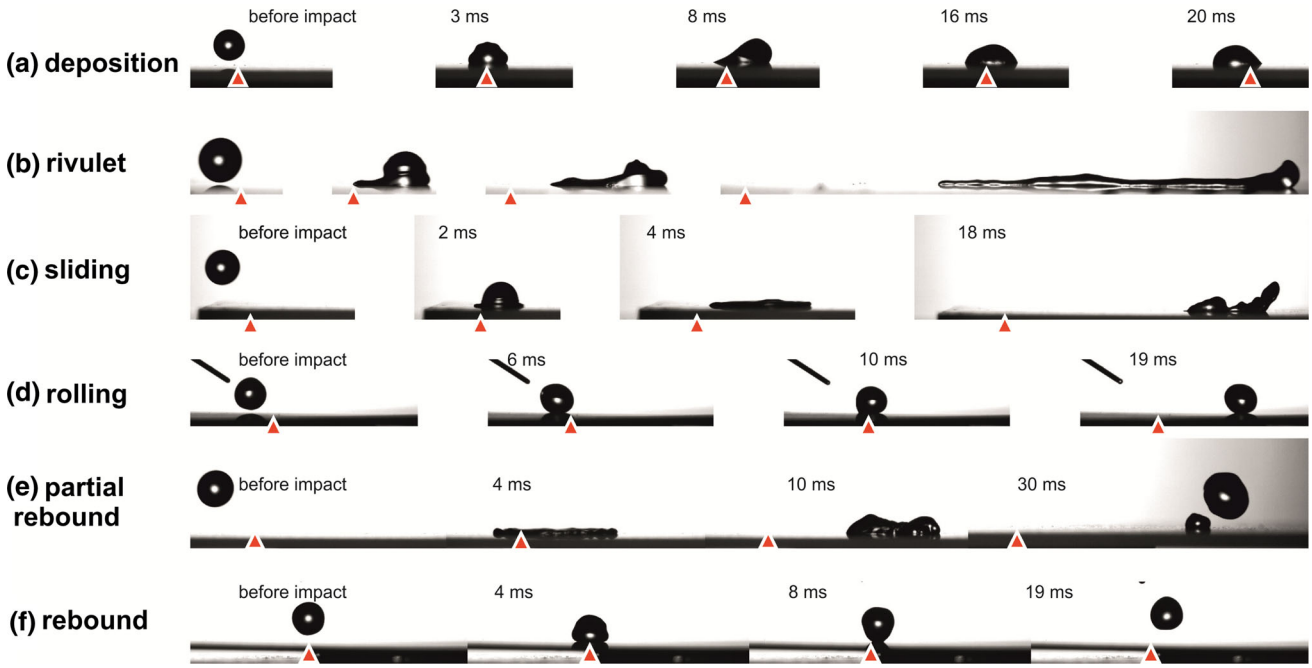

Fig. 3 Outcomes of water drop impact onto various tilted substrates: **a** deposition on A1-Teflon ($V < 0.1$ m/s, $\alpha = 45°$); **b** rivulet on A1-Teflon ($V = 2.36$ m/s, $\alpha = 80°$); **c** sliding on A1-Teflon ($V = 2.36$ m/s, $\alpha = 60°$); **d** rolling on SHS-1 ($V < 0.1$ m/s, $\alpha = 60°$); **e** partial rebound on A1-Teflon ($V = 2.36$ m/s, $\alpha = 45°$); **f** rebound on SHS-1 ($V < 0.1$ m/s, $\alpha = 10°$). The *triangle* in each image indicates the location of the impact point

(a) *Deposition*, when the whole drop remains stuck close to the impact point. This regime corresponds to the so-called "spread" in Šikalo et al. (2005a, b).

(b) *Rivulet*, when the drop slides downhill while spreading, recoil does not occur, and $D_{//}$ increases continuously while drop flows downhill; the uphill contact point may either remain pinned on the surface or partially move downstream, as shown in Fig. 3b.

(c) *Sliding*, when the entire drop (thus, including both uphill and downhill contact points edge) moves downhill and, at the end of the recoil phase, $D_{//}$ remains constant while drop slides, typically with $D_{//}/D_0$ greater than ~ 1, and the entire liquid mass (i.e., the main part plus possible tiny secondary droplets) remains attached to the surface.

(d) *Rolling*, when the drop rolls downhill, typically preserving high contact angles and thus a reduced contact area, i.e., with $D_{//}/D_0 \ll 1$.

(e) *Partial rebound*, when a part of the drop pinches off from the surface, while the other remains stuck (and eventually flows downhill afterward).

(f) *Rebound* (or complete rebound), when the entire drop detaches from the surface.

Other known phenomena, such as prompt splash (typically on the downhill advancing front), or drop breakup, were observed in combination with the above-described outcomes, in particular on superhydrophobic surfaces. Prompt splash is indeed a typical outcome for drop impact on rough surfaces (Rioboo et al. 2001). The phenomenon known as impalement (see Fig. 2), typically prevents the drop from fully rebounding from the surface, causing the drop to partially rebound or to remain deposited on the surface.

The time evolution of $D_{//}$, made non-dimensional by D_0, at different tilt angles is illustrated in Fig. 4a, for one representative surface, A1-Teflon. Figure 4b illustrates the x-coordinate evolution of the uphill and downhill contact points, x_{uphill} and x_{downhill}, respectively, where the relation between contact diameter and contact point position is $D_{//} = x_{\text{downhill}} - x_{\text{uphill}}$. In the case complete rebound occurred (for $\alpha = 10°$ and $30°$), the contact diameter $D_{//}$ initially increased and, after reaching the maximum value (maximum spreading) decreased to zero, when the drops lifted-off from the surface. In the sliding regime ($\alpha = 45°$), drop initially spread, up to the point when $D_{//}$ reached a maximum, then partially recoiled, and finally slid downstream with a constant contact diameter $D_{//}$. Differently, in the rivulets regime (for $\alpha = 70°$), $D_{//}$ increased continuously, while drop slid downhill, without recoiling.

3.2 Smooth hydrophobic surface: A1-Teflon

Water drop impacts on the smooth hydrophobic tilted surface, A1-Teflon, showed four different impact

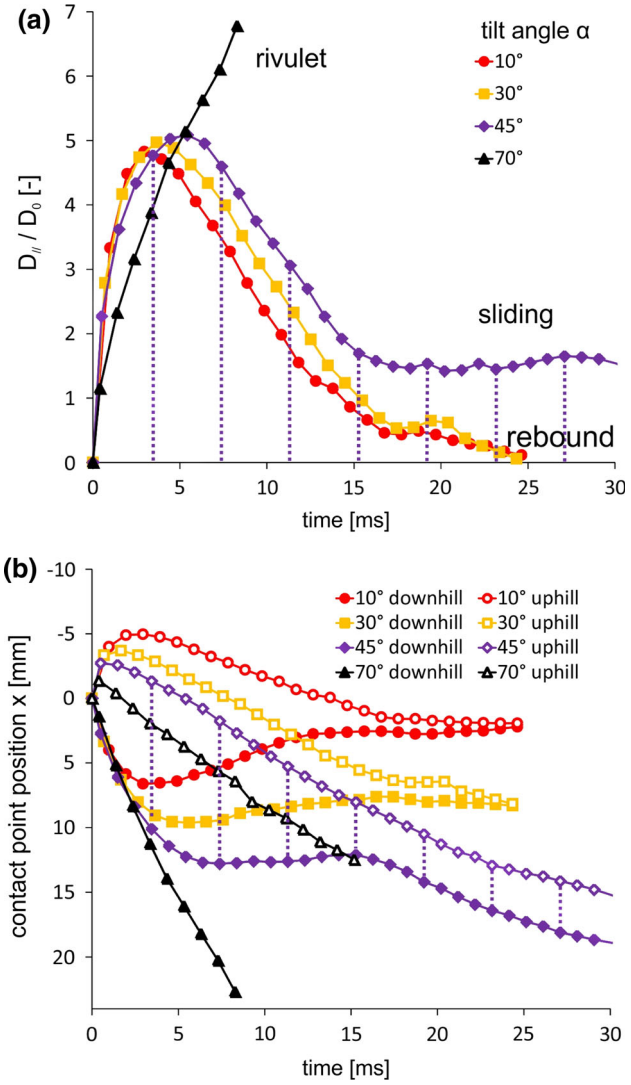

Fig. 4 Time evolution of **a** the non-dimensional contact diameter $D_{//}/D_0$ and **b** uphill and downhill contact point position, x_{uphill} and x_{downhill}, respectively, for different tilt angles α on A1-Teflon surface (single runs). Impact conditions are: drop velocity $V = 3.1$ m/s, drop diameter $D_0 = 2.57$ mm, Weber number $We = 339$. Different regimes can be identified: drop rebound ($\alpha = 10°$ and 30°), sliding drop ($\alpha = 45°$), and rivulet ($\alpha = 70°$). *Vertical dotted lines* highlight (for $\alpha = 45°$) highlight that $D_{//} = x_{\text{downhill}} - x_{\text{uphill}}$

outcomes: rebound, partial rebound, sliding, and rivulets (as defined in Fig. 3). The drop impact outcome map is illustrated in Fig. 5, where different outcomes are identified on the *We*–α plane, for water drops impacting on A1-Teflon. By increasing both *We* and α, i.e., moving from bottom-left to top-right in Fig. 5, the drop outcome progressively changes from drop rebound to an intermediate condition where sliding and partial rebound occurred, and finally to rivulets, which appears at the highest surface tilt. The map shows that drop rebound occurred at all tested Weber numbers for $\alpha \leq 10°$. By increasing α, a critical Weber number, We_C, above which drop did not rebound

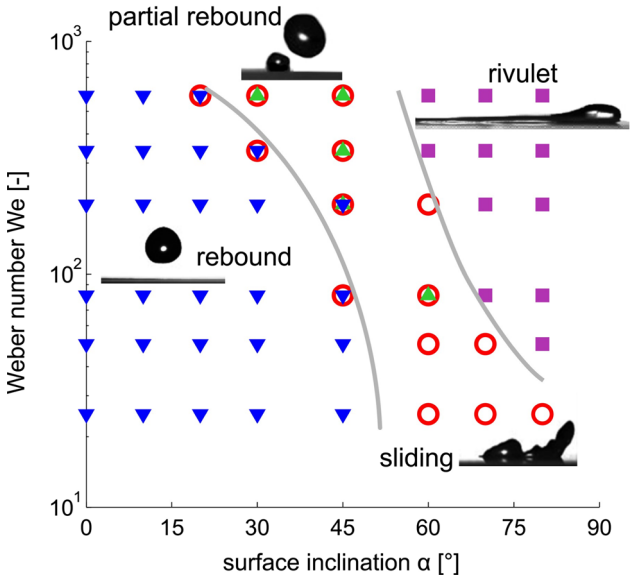

Fig. 5 Drop impact outcome map for the hydrophobic surface A1-Teflon. The outcomes observed on hydrophobic surfaces are rebound (*blue triangles*), partial rebound (*green triangles*), sliding (*red open circles*), and rivulets (*violet squares*). *Gray lines* are used to indicate the transition between different regimes

can be identified. In particular, the We_C decreased by increasing the tilt angle, α. For $\alpha > 45°$, drop rebound was never observed on A1-Teflon surface.

3.3 Drop impacts on SHS-1

On the SHS-1 surface, complete rebound was observed for all impact conditions, i.e., for $25 < We < 585$ and surface tilt angle $0° < \alpha < 80°$. Rolling of the drop down the surface was observed only when the drop was gently deposited on the surface, with almost zero velocity. Figure 6 illustrates the values of drop rebound time, t_R, as function of surface tilt angle, α, at different impact Weber numbers. Two different trends were recognized: at high Weber numbers ($We \geq 199$), surface tilt had a positive effect on drop rebound, with a reduction in drop rebound time from $\sim$16 ms (for $\alpha = 0°$) to values of $\sim$9 ms (for $\alpha = 80°$), corresponding to $\sim$40 % lower rebound time at the highest tilt. For the three lowest values of tested Weber numbers ($We \leq 81$), however, rebound time initially decreased from small tilt angles, but then increased at higher values of tilt angle. The reduction in the rebound time can be qualitatively explained looking at the kinematics of the uphill and downhill contact points, illustrated in Fig. 7, in particular during the recoil phase. The time at which maximum spreading is reached increases slightly by increasing the tilt angle α (see Fig. 7a). It is interesting to note that in the initial phases of spreading (from 0 to 3 ms) the curves for x_{downhill} are almost overlapped (see Fig. 7b), meaning that

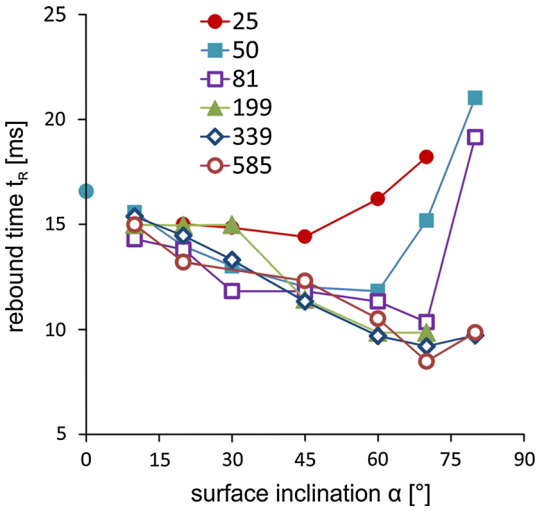

Fig. 6 Drop rebound time on SHS-1 surface as function of tilt angle, α, at different Weber numbers (see legend). Standard deviation for rebound time is ± 1.5 ms. The value indicated at $\alpha = 0°$ corresponds to the rebound time from the correlation by Richard et al. (2002)

despite the tangential velocity, V_T, is increasing, the downhill contact point moves with similar speed. After maximum spreading is reached, recoil occurs: data in Fig. 7 show that the uphill contact point velocity increases by increasing the tilt angle α, so that the recoil process becomes faster and faster, leading overall to reduction in the rebound time. In the other hand, the increase in rebound time at lowest *We* numbers can be attributed to the reduction in normal impact velocities, V_N, which reduces to values in the order of 0.1 m/s at highest tilt. Indeed, Okumura et al. (2003) showed that for normal impacts at low impact speed, i.e., $V < 0.20$ m/s, the rebound time increased typically by factor up to 2: this variation in the rebound time was attributed to gravity effects which affect drop rebound for small deformations.

Figure 7a, b illustrates the time evolution of $D_{//}/D_0$ and of contact points for impacts at different tilt angle on SHS-1, to provide a direct comparison between drop dynamics on SHS-1, which is a superhydrophobic surface, and on A1-Teflon, which is a smooth hydrophobic surface (see Fig. 4). The major difference between the two surfaces is the effect of the tilt angle: on SHS-1, drop rebound always occurred at any tilt angle; also, increasing the tilt angle helped reducing drop rebound time, facilitating drop rebound and shedding from the surface. Differently, on a smooth hydrophobic surface, no rebound was observed above a certain surface tilt angle, i.e., $\alpha > 45°$, and drop remained partially or totally stuck on the substrate. A comparison of data from Figs. 4 and 7 allows to understand the effect of wettability, especially in the recoiling phase, which is faster on the superhydrophobic surface.

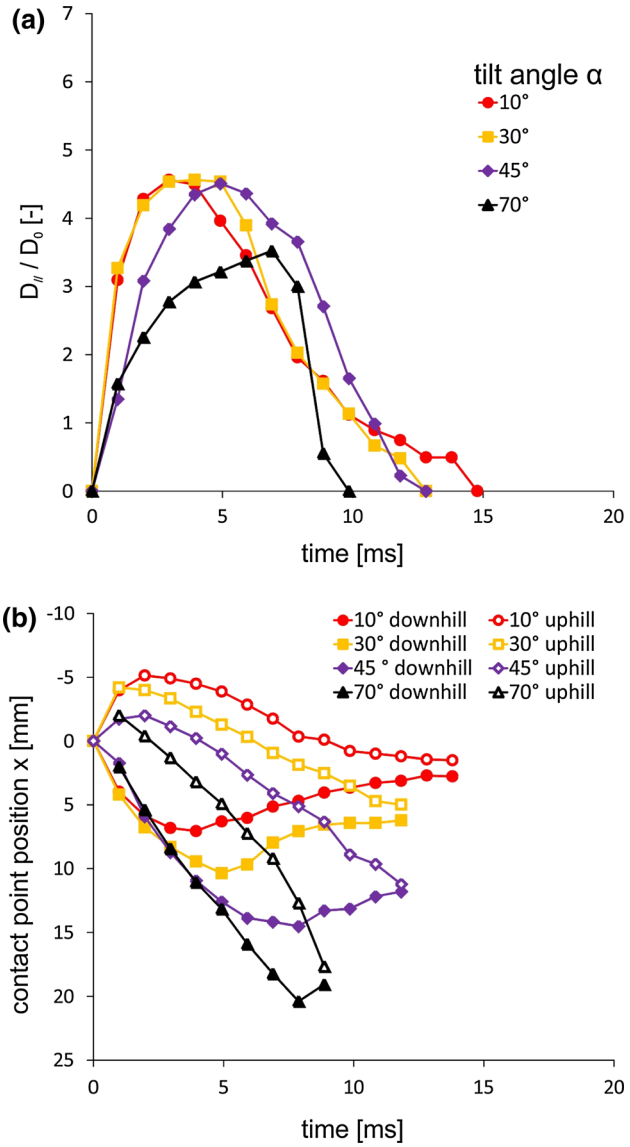

Fig. 7 Time evolution of **a** the non-dimensional contact diameter $D_{//}/D_0$ and **b** uphill and downhill contact point positions for different tilt angle α on SHS-1 surface. Impact conditions are: drop velocity $V = 3.1$ m/s, drop diameter $D = 2.57$ mm, Weber number $We = 339$. In all cases, drop rebound from the surface after impact

Differences in the maximum spreading become even clearer in the spreading phase for moderate *We* regime ($We < 200$), as already addressed in a previous work (Antonini et al. 2012), where millimetric water drops were also investigated.

In Fig. 8, the quantity $L_{//}/t_{rebound}$ was plotted as a function of the tangential impact velocity, V_T, for the superhydrophobic surfaces SHS-1 and for two different impact velocity, V (1.7 and 3.3 m/s). $L_{//}$ is the distance traveled by the drop while in contact with the surface (see Fig. 2). As such, the ratio $L_{//}/t_{rebound}$, which is dimensionally a velocity, provides an indication of the drop average

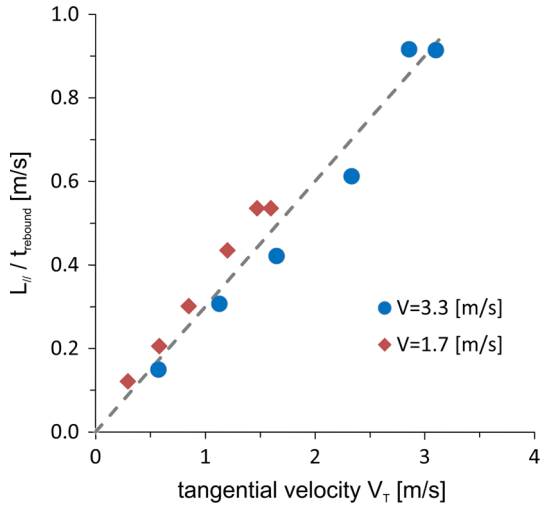

Fig. 8 $L_{//}/t_{\text{rebound}}$ as a function of the tangential impact velocity, V_T, for the superhydrophobic surfaces SHS-1. $L_{//}$ is the distance traveled by the drop while in contact with the surface (see Fig. 1). *Dotted line* represents data best linear fitting. *Line slope* is 0.3

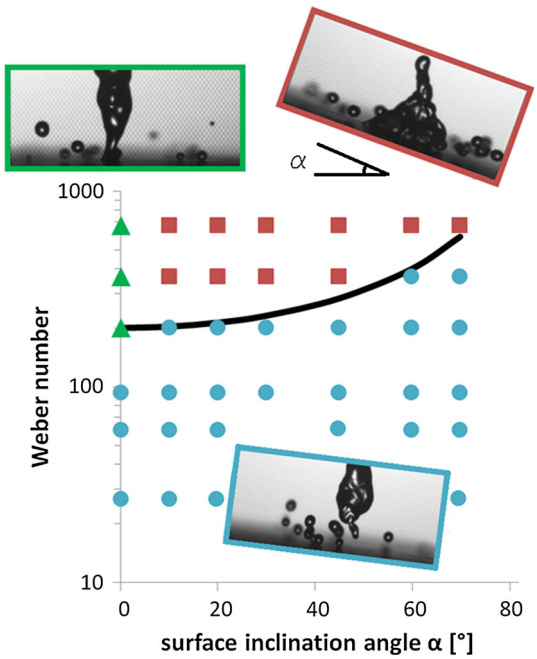

Fig. 9 Drop impact outcome map for the superhydrophobic surface SHS-2. The outcomes observed on SHS-2 surfaces are: rebound (*blue circles*), impalement on surface with partial rebound and sticky drop on the surface (*green triangles*), and impalement on surface with rebound and no sticky drop on the surface (*red squares*). For $\alpha = 0°$ (normal impact), complete rebound occured up to $We = 200$; for higher We, impalement occurred and part of the drop remained attached to the substrate. The *black line* corresponds to drop impacts with normal Weber number $We_N = 200$

flowing speed, while in contact with the surface. Data in Fig. 8 clearly show that $L_{//}/t_{\text{rebound}}$ is linearly proportional to the tangential impact velocity, V_T. In particular, best fitting of the experimental data give $L_{//}/t_{\text{rebound}} = 0.3\ V_T$.

3.4 Drop impalement on SHS-2

On the SHS-2, complete rebound was observed for normal impacts ($\alpha = 0°$) only for Weber numbers lower than a critical Weber number $We_C \approx 200$ (see Fig. 9). For higher Weber numbers, impalement occurred and only a partial rebound was observed: most of the liquid rebounded from the surface, but a small secondary drop remained attached to the surface, in the area around the impact point. This is due to meniscus penetration in the surface topography, as discussed above. It is noticeable that SHS-2 has lower resistance to impalement compared with SHS-1, although SHS-2 would be classified as a better superhydrophobic surface based on contact angle measurements, since it has higher contact angles and lower contact angle hysteresis.

Note that the reason why on SHS-1 and SHS-2 surfaces impalement occurs at a different velocity is due to a different surface capillary pressure, p_c, which resists meniscus penetration. Capillary pressure is in general a complex function of surface chemistry and topography and can be a priori defined on special surfaces with clearly defined geometry, such as micro-pillar surfaces. On superhydrophobic surfaces with random roughness, such as chemically etched superhydrophobic surfaces used in the present study, capillary pressure can be estimated a posteriori. As shown recently by Maitra et al. (2014), surface capillary pressure, p_c, scales with the maximum pressure in the gas before the drop touches the substrate, $p_{\max}$, which can be computed as $p_{\max} = \frac{0.88\left(R\mu_g^{-1}V^7\rho^4 Ca\right)^{1/3}}{St^{4/9}}$ (Mandre et al. 2009). R is the drop radius, μ_g is the air viscosity, V impact velocity, ρ is the liquid density, $Ca = \mu_g V/\sigma$ is the capillary number, and $St = \mu_g/\rho VR$ is the Stokes number. Data for micro-pillar textured surfaces (Maitra et al. 2014) showed that $p_{\max} = kp_c$, where the constant k was found experimentally to be equal to 80. Based on our tests, we can estimate the capillary pressure for SHS-2 to be $p_c = 61$ kPa (where critical velocity was $V_c = 2.4$ m/s). For SHS-1, the critical velocity was higher that the experimental limit for our apparatus, leading to the conclusion that the capillary pressure for SHS-1 is $p_c > 320$ kPa (being $V_c > 4.1$ m/s). For normal impacts, the impalement region on SHS-2 could be identified since the $D_{//}$ at the solid–liquid interface did not reduce to zero, as in case of drop rebound. When the contact line reached the impaled area, contact line remained pinned and the contact angle decreased to values much lower than 90°. This is typical for transition from Cassie–Baxter to Wenzel wetting state (see Fig. 1). With respect to oblique impacts ($\alpha > 0°$), two different outcomes were observed (see

Fig. 9): when the normal Weber number, We_N, was lower than the critical value identified for normal impacts (i.e., $We_N < We_C \approx 200$), drop spread on the surface and complete rebound occurred without impalement, while the drop slid downhill. For $We_N > 200$, drop impalement occurred, as shown by the fact that the dynamic receding angle contact angle reached values lower than 90° on the uphill front. Nonetheless, complete rebound occurred.

To conclude, experimental results show that for oblique impacts on SHS-2, the normal Weber number, We_N, (i.e., the normal velocity component V_N) is the parameter that control impalement transition. In addition, surface tilt has a positive effect on drop shedding, since even for low tilt angles the water drops rebounded completely from the surface and no secondary drops remained attached to the substrate, as de-wetting of the impaled area was possible.

4 Conclusions

A study on water drop impacts on tilted surfaces with different wettability, from hydrophobic to superhydrophobic surfaces, was conducted, performing a phenomenological investigation of drop impact outcomes and addressing the conditions for drop rebound. The analysis allowed identification of six different impact outcomes: deposition, rivulet, sliding, rolling, partial rebound, and rebound. Drop impact image analysis led to two main findings: for drop impact on superhydrophobic surfaces, surface tilting facilitated drop rebound from a surface and allowed a reduction in rebound time up to 40 %; on the tested hydrophobic surface, the increase in both surface tilting and impact Weber number led to a transition from drop rebound, to partial rebound and sliding, and finally to rivulet. On one tested superhydrophobic surface, drop rebound occurred in all tested condition. Differently, on the second tested superhydrophobic surface, despite having higher contact angles and lower contact angle hysteresis, impalement occurred above a critical *We* number, and transition from a complete to a partial rebound was observed. When tilting the surface, impalement always occurred at the same critical normal Weber number, We_N, computed using the normal velocity, V_N. However, we observed that surface tilting had a positive effect on drop shedding from the surface, allowing the de-wetting of the impaled area and thus drop rebound from the surface.

Acknowledgments The authors acknowledge Regione Lombardia for funding the project "*Strumenti innovativi per il progetto di sistemi antighiaccio per l'aeronautica*" (within the Framework Agreement) and Alenia Aermacchi for financial support. CA acknowledges funding by a Marie Curie Intra-European Fellowship, within the 7th European Community Framework Programme (ICE^2, 301174). The authors also thank I. Bernagozzi and I. Malavasi (University of Bergamo), H. Chen (University of Alberta, Canada) and A. Amirfazli (University of York, Canada) for sample preparation. CA acknowledges Daniele Foresti (ETH Zurich) for helpful discussions.

References

Abuku M, Janssen H, Poesen J, Roels S (2009) Impact, absorption and evaporation of raindrops on building facades. Build Environ 44:113–124

Antonini C, Innocenti M, Horn T, Marengo M, Amirfazli A (2011) Understanding the effect of superhydrophobic coatings on energy reduction in anti-icing systems. Cold Reg Sci Technol 67:58–67

Antonini C, Amirfazli A, Marengo M (2012) Drop impact and wettability: from hydrophilic to superhydrophobic surfaces. Phys Fluids 24:102104

Antonini C, Bernagozzi I, Jung S, Poulikakos D, Marengo M (2013a) Water drops dancing on ice: how sublimation leads to drop rebound. Phys Rev Lett 111:014501

Antonini C, Villa F, Bernagozzi I, Amirfazli A, Marengo M (2013b) Drop rebound after impact: the role of receding contact angle. Langmuir 29:16045–16050

Antonini C, Lee JB, Maitra T, Irvine S, Derome D, Tiwari MK, Carmeliet J, Poulikakos D (2014) Unraveling wetting transition through surface textures with X-rays: liquid meniscus penetration phenomena. Sci Rep 4:4055

Bartolo D, Bouamrirene F, Verneuil É, Buguin A, Silberzan P, Moulinet S (2006) Bouncing or sticky droplets: impalement transitions on superhydrophobic micropatterned surfaces. Europhys Lett 74:299–305

Bhushan B, Jung YC, Koch K (2009) Micro-, nano- and hierarchical structures for superhydrophobicity, self-cleaning and low adhesion. Phil Trans R Soc A 367:1631–1672

Dewitte J, Berthoumieu P, Lavergne G (2011) Drop impact on a heated wall—influence of ambient pressure. Proceedings of 24th ILASS Europe conference, Estoril, Portugal, September 2011

Huanchen C, Tang T, Amirfazli A (2012) Fabrication of polymeric surfaces with similar contact angles but dissimilar contact angle hysteresis. Colloid Surf A 408:17–21

Li W, Amirfazli A (2005) A thermodynamic approach for determining the contact angle hysteresis for superhydrophobic surfaces. J Colloid Interface Sci 292:195–201

Li N, Zhou Q, Chen X, Xu T, Hui S, Zhang D (2008) Liquid drop impact on solid surface with application to water drop erosion on turbine blades, part I: nonlinear wave model and solution of one-dimensional impact. Int J Mech Sci 50:1526–1542

Liu Y, Chen X, Xin JH (2009) Can superhydrophobic surfaces repel hot water? J Mater Chem 19:5602–5611

Maitra T, Tiwari MK, Antonini C, Schoch P, Jung S, Eberle P, Poulikakos D (2014) On the nanoengineering of superhydrophobic and impalement resistant surface textures below the freezing temperature. Nano Lett 14(1):172–182

Mandre S, Mani M, Brenner MP (2009) Precursors to splashing of liquid droplets on a solid surface. Phys Rev Lett 102:13

Mao T, Kuhn DCS, Tran H (1997) Spread and rebound of liquid droplets upon impact on flat surfaces. AIChE J 43:2169–2179

Marengo M, Antonini C, Roisman IV, Tropea C (2011) Drop collisions with simple and complex surfaces. Curr Opin Colloid Interface Sci 16:292–302

Okumura K, Chevy F, Richard D, Quéré D, Clanet C (2003) Water spring: a model for bouncing drops. Europhys Lett 62:237–243

Papadopoulos P, Mammen L, Deng X, Vollmer D, Butt HJ (2013) How superhydrophobicity breaks down. Proc Natl Acad Sci USA 110(9):3254–3258

Pasandideh-Fard M, Aziz SD, Chandra S, Mostaghimi J (2001) Cooling effectiveness of a water drop impinging on a hot surface. Int J Heat Fluid Fl 22:201–210

Quéré D (2005) Non-sticking drops. Rep Prog Phys 68:2495

Reyssat M, Pèrin A, Marty F, Chen Y, Quéré D (2006) Bouncing transitions in microtextured materials. Europhys Lett 74:306–312

Richard D, Clanet C, Quéré D (2002) Contact time of a bouncing drop. Nature 417:811

Rioboo R, Marengo M, Tropea C (2001) Outcomes from a drop impact on solid surfaces. Atomization Spray 11:155–165

Rioboo R, Voué M, Vaillant A, De Coninck J (2008) Drop impact on porous superhydrophobic polymer surfaces. Langmuir 24:14074–14077

Rioboo R, Delattre B, Duvivier D, Vaillant A, De Coninck J (2012) Superhydrophobicity and liquid repellency of solutions on polypropylene. Adv Colloid Interface Sci 175:1–10

Schiaffino S, Sonin AA (1997) Molten droplet deposition and solidification at low Weber numbers. Phys Fluids 9:3172–3187

Šikalo Š, Tropea C, Ganić EN (2005a) Dynamic wetting angle of a spreading droplet. Exp Therm Fluid Sci 29:795–802

Šikalo Š, Tropea C, Ganić EN (2005b) Impact of droplets onto inclined surfaces. J Colloid Interface Sci 286:661–669

Yarin AL (2006) Drop impact dynamics: splashing, spreading, receding, bouncing. Annu Rev Fluid Mech 38:159–192

Zhou Q, Li N, Chen X (2008) Liquid drop impact on solid surface with application to water drop erosion on turbine blades, part II: axisymmetric solution and erosion analysis. Int J Mech Sci 50:1543–1558